

Data-driven discretization: a method for systematic coarse graining of partial differential equations

Yohai Bar-Sinai,^{1,*} Stephan Hoyer,^{2,†} Jason Hickey,² and Michael P. Brenner¹

¹*School of Engineering and Applied Sciences, Harvard University, Cambridge, MA*

²*Google Research, Mountain View, CA*

Many problems in theoretical physics are centered on representing the behavior of a physical theory at long wave lengths and slow frequencies by integrating out degrees of freedom which change rapidly in time and space. This is typically done by writing effective long-wavelength governing equations which take into account the small scale physics, a procedure which is very difficult to perform analytically, and sometimes even phenomenologically. Here we introduce *data driven discretization*, a method for automatically learning effective long-wavelength dynamics from actual solutions to the known underlying equations. We use a neural network to learn a discretization for the true spatial derivatives of partial differential equations. We demonstrate that this approach is remarkably accurate, allowing us to integrate in time a collection of nonlinear equations in one spatial dimension at resolutions 4-8x coarser than is possible with standard finite difference methods.

The solutions of nonlinear partial differential equations can have enormous complexity, with nontrivial structure over a large range of length and timescales. Developing effective theories that integrate out behavior on short length scales and timescales is the goal of many successful physical theories. As examples, geometric optics is an effective theory of Maxwell equations at scales much longer than the light’s wavelength and times much slower than its period [1]; Density Functional Theory models the full many-body quantum wavefunction using a much lower dimensional object – the electron density field [2]; and the effective diffusivity and viscosity of a turbulent fluid flow parameterize the effect of small scale features on large scale behavior [3]. These models derive the coarse-grained dynamics by more or less systematic integration of the underlying governing equations (by using, respectively, Migdal-Kadanoff technique, WKB theory, Local Density Approximation and a closure relation for the Reynold stress). The gains from such a systematic coarse graining are, of course, enormous. Conceptually, it allows a deep understanding of emergent phenomena that would otherwise be masked by irrelevant details, and practically, it allows computation of vastly larger systems for much longer times.

The procedure of averaging out unresolved degrees of freedom invariably consists of replacing them by an effective terms or parameters that mimic their typical behavior. In other words, one seeks to identify the salient features of the dynamics at short-and-fast scales and to replace the detailed dynamics by terms that have a similar average effect on the long-and-slow scales. Deriving reliable effective equations is often challenging, especially for practical problems which are typically inhomogeneous [4].

In this work we introduce *data-driven discretization*, an automated approach for performing this crucial coarse graining step. Our basic idea derives from recent advances in machine-learning algorithms, which have become extraordinarily efficient at identifying recurrent patterns in data and producing generative models for these patterns. We use these techniques to produce discretizations for nonlinear partial differential equations (PDEs) that effectively coarse grain over smaller scales. This approach is qualitatively different from coarse graining techniques that are currently in use. Instead of analyzing the equations of motion to derive the effective behavior of the fast and short scales, we directly learn from high resolution solutions to these equations.

Several related approaches for computationally extracting effective dynamics have been used in the past. Kevrekidis and collaborators introduced equation-free modeling as a method that “bypasses the derivation of macroscopic evolution equations when these equations conceptually exist but are not available in closed form” [5]. This is achieved by choosing proper initial conditions for the fine-scale variables based on the coarse-scale ones and evaluating the derivative of the latter based on integrating the former. This method has similar spirit to our approach, but it does not learn the fine-scale dynamics and use the memorized statistics in subsequent times to reduce the computational load. Dynamic Mode Decomposition [6, 7] finds the optimal linear operator that approximates observed non-linear dynamics, thereby extracting a slow dynamic manifold. But these modes are situation dependent, and does not lead to a robust coarse graining. Schmidt and Lipson [8] and Brunton *et. al.* [9] have developed ways to learn governing equations from dynamics, but only if these equations are assumed to be drawn from some predefined dictionary.

More recently, a number of works have applied modern machine learning techniques to the study of partial differential equations. These works have focused either on speed [10–13] or recovering unknown dynamics [9, 14]. Models focused on speed often replace the slowest com-

* ybarsinai@gmail.com; YBS and SH contributed equally to this work

† shoyer@google.com; YBS and SH contributed equally to this work

ponent of a physical model with machine learning, e.g., the solution of Poisson’s equation in incompressible fluid simulations [11] or sub-grid cloud models in climate simulations [12]. Another approach is to build reduced order models that approximate dynamics in a lower dimensional space [10, 15, 16]. These approaches are appealing for control, but the learned models may have limited generalization beyond the boundary conditions for which they were trained. Alternatively, models could be used to add high-resolution detail on top of low-accuracy simulations after the fact [13]. An important development is the ability to guarantee that some physical constraints are satisfied exactly by plugging learned components into a fixed equation of motion. For example, valid fluid dynamics can be guaranteed by learning either velocity fields directly [14] or a vector potential for velocity in the case of incompressible dynamics [10].

Most closely related to this work, it has recently been shown that neural networks can be used to calculate closure conditions for coarse grained turbulent flow models [17, 18]. However, these models rely on existing coarse-grained schemes specific to turbulent flows (Reynolds Averaged Navier Stokes, Large Eddy Simulation) and do not discretize the equations directly.

DATA DRIVEN SUB-GRIDSCALE MODELING OF PDES

Consider a generic PDE, describing the evolution of a continuous field $v(x, t)$

$$\frac{\partial^n v}{\partial t^n} = F\left(t, x, v, \frac{\partial v}{\partial x_i}, \frac{\partial v}{\partial x_i \partial x_j}, \dots\right). \quad (1)$$

Most PDEs in the exact sciences can be cast in this form, including equations that describe hydrodynamics, electrodynamics, chemical kinetics and elasticity. A common algorithm for numerically solving such equations is the method of lines [19]: the field v is represented by its values, $v_1(t) \dots v_N(t)$ at a discrete set of node points x_1, \dots, x_N . The time evolution of v_i can be computed directly from Eq. (1) by approximating the spatial derivatives at the node points. There are various methods for creating this approximation – finite difference, Galerkin projection, spectral differentiation, etc. – all yielding formula resembling

$$\frac{\partial^n v}{\partial x^n} \approx \sum_i \alpha_i^{(n)} v_i, \quad (2)$$

where the $\alpha_j^{(n)}$ are precomputed coefficients. For example, the one dimensional (1D) finite difference approximation for $\frac{\partial v}{\partial x}$ to first-order accuracy is

$$\frac{\partial v}{\partial x} \Big|_{x=x_i} \approx \frac{v_{i+1} - v_i}{\Delta x} + \mathcal{O}(\Delta x) \quad (3)$$

where $\Delta x = x_i - x_{i-1}$ is the spatial resolution. While sophisticated methods of alternating between different

finite-difference schemes according to local rules also exist [20, 21], standard finite-difference schemes use one set of pre-computed coefficients for all points in space. This discretization transforms Equation 1 into a set of coupled ordinary differential equations (ODEs) of the form

$$\frac{\partial^n v_i}{\partial t^n} = F(t, x, v_1, \dots, v_N), \quad (4)$$

that can be numerically integrated using standard techniques. The accuracy of the solution to Eq. (4) depends on Δx , converging to a solution of Eq. (2) as $\Delta x \rightarrow 0$. Qualitatively, accuracy requires that Δx is smaller than the spatial scale of the smallest feature of the field $v(x, t)$.

However, the scale of the smallest features is often orders of magnitude smaller than the system size. For problems in three spatial dimensions, the required number of points increases like the cube of the spatial resolution. Resolving the solution becomes computationally unfeasible, and indeed a primary driver of high performance computing has been the ever increasing need to accurately resolve smaller scale features in partial differential equations. Even with petascale computational resources, the largest direct numerical simulation of a turbulent fluid flow ever performed has Reynolds number of order 1,000, using about 5×10^{11} grid points [22–24]. Simulations (e.g., at higher Reynolds number) can only be done by replacing the physical equations with effective equations that model unresolved physics. These equations are then discretized and solved numerically using e.g., the method of lines. This overall procedure essentially modifies Eq. (2), by changing the weights α_i to model unresolved physics, replacing the discrete equations in Eq. (4) with a different set of discrete equations.

The main idea of this paper is that the unresolved physics can instead be learned directly from the data. That is, instead of deriving an approximate coarse-grained continuum model and discretizing it, we suggest to directly learn the low-resolution discrete model that encapsulates the unresolved physics.

Intuitively, the space of solutions to a given equation live on a manifold that is much smaller than the space of all possible functions, as illustrated by the fact that even complicated PDEs generate patterns that repeat themselves again and again. If we only knew the solution manifold we could generate *equation specific* approximations for the spatial derivatives in Eq. (2), approximations that have the potential to hold even when the system is under resolved. In contrast to the standard numerical methods which use a single fixed set of coefficients at all points in space, the coefficients $\alpha_j^{(n)}$ we obtain are now equation-dependent and data-dependent in the sense that different regions in space (i.e., inside and outside a shock) will use different coefficients. To discover these formulae, we use machine learning: we first generate a training set of high resolution data, and then learn the discrete approximations to the derivatives in Eq. (2) from this dataset. This produces a trade off in computational cost: we carry

out high resolution simulations on small systems to develop local approximations to the solution manifold of the PDE, and then use these approximations to solve the equations in much larger systems at significantly reduced spatial resolution.

BURGERS' EQUATION

For concreteness, we demonstrate this approach with a specific example in one spatial dimension. Burgers' equation is a simple nonlinear equation which models shock formation:

$$\frac{\partial v}{\partial t} = -v \frac{\partial v}{\partial x} + \eta \frac{\partial^2 v}{\partial x^2} + f(x, t), \quad (5)$$

where $\eta > 0$ is the viscosity and $f(x, t)$ is an external forcing term. For generic initial conditions, solutions of Burgers' equation spontaneously develops sharp shocks, with specific relationships between the shock height, width and velocity that define the solution manifold of the equation.

With this in mind, consider a typical segment of the solution (Fig. 1). We would like to compute the time derivative of the field given a discrete set of n points around x_0 (orange points in Fig. 1). Standard finite difference formulas predict this time derivative by approximating v as a polynomial of degree $n-1$, passing through the given n points (green curves in Fig. 1). But solutions to Burger's equations are not just any polynomials, they are shocks with characteristic properties. By using this information, we can derive a more accurate, albeit equation specific, formula for the spatial derivatives.

To demonstrate this explicitly, we ran many simulations of Eq. (5) and used the resulting data to train a regressor. Fig. 1 shows the result of Support Vector Regression (SVR) trained on 30,000 line segments (details in methods/SI). The figure shows four example segments; within each segment we use the values of the function at five equally spaced node points (colored orange) to approximate the spatial derivatives. The regression (SVR) is far superior to the polynomial approximation, able to parameterize the solution manifold with sparsely sampled points. This clearly demonstrates that, given enough training data, the spatial resolution needed in order to parametrize the solution manifold can be greatly reduced if one uses equation-specific approximation rather than agnostic schemes like finite differences.

The natural question to ask next is whether we can now use this parametrization to integrate equations in time. This presents two major additional challenges: numerical stability and generalizability. Numerical stability is a shared concern with classical numerical methods: small but consistent errors (bias) can accumulate in time due to inexact approximations. Generalizability is a related but distinct concern: our models should still give accurate results even when presented with examples very unlike

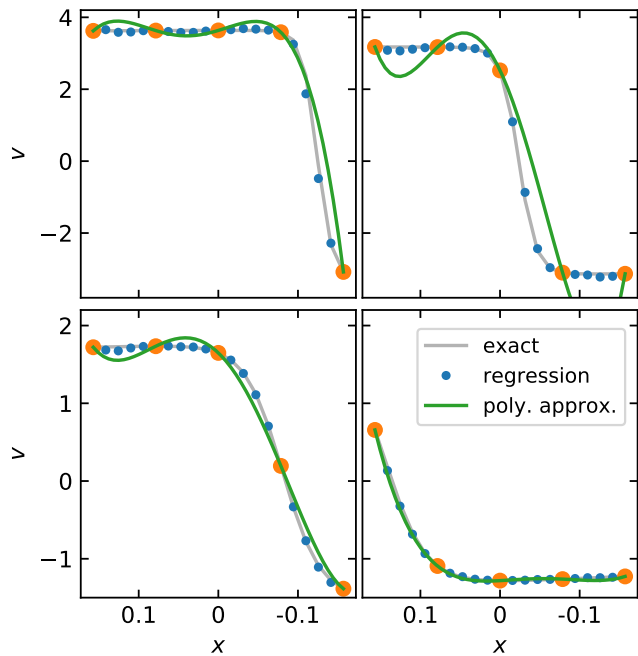


FIG. 1. A few typical segments of solutions to Burgers' equation. Based on the five orange points we interpolate either by polynomial interpolation (green line) or by regression (blue points). The latter evidently outperforms the former. The parameters of the equation are given in the methods section.

anything they saw as part of model training. Accordingly, we decided to pursue an approach based on multi-layer neural networks, because of their flexibility, including their scalability to large datasets and the ability to impose physical constraints and interpretability through choice of model architecture.

The high-level aspects of the network's design, which we believe are of general interest, are described below. Additional technical details are available in the Methods Section and the complete source code is freely available online [25].

General structure The model is a fully-convolutional neural network [26]. We use the exact same architecture (three layers, each with 32 filters of size five, ReLU non-linearity) for coarse-graining all equations discussed in this work.

Conservative constraint Like many PDEs of fluid dynamics, Burgers' equation can be written explicitly in the form of a continuity equation, i.e., the temporal derivative is given as a divergence of a flux J :

$$\frac{\partial v}{\partial t} = \frac{\partial}{\partial x} J(v) + f(x, t), \quad J \equiv -\frac{v^2}{2} + \eta \frac{\partial v}{\partial x} \quad (6)$$

We found that a major increase in stability is obtained when the prediction is done in a three-step process: first, the network predicts the value of the spatial derivatives on a staggered grid, i.e., between grid points. Then, these derivatives are used to calculate the flux J , still on the staggered grid. Third, the temporal derivative on the

original grid is obtained by differentiating J using the standard finite-difference formula Eq. (3).

This formulation, in the style of a Finite Volume Method [27], ensures the coarse-grained solution satisfies the conservation law defined by the continuity equation. It results in significantly more stable behavior when integrating over time.

Pseudo-linear representation The manner with which the network attempts to predict the spatial derivatives is a generalized finite-difference formula of type of Eq. (2). That is, the output of the network is a list of coefficients $\alpha_1, \dots, \alpha_N$ such that the ℓ -th derivative is given by

$$\left. \frac{\partial^\ell v}{\partial x^\ell} \right|_{x=x_0} = \sum_{i=1}^N \alpha_i v(x_i) \quad (7)$$

where the x_i are N neighboring points. This means that our model is a “pseudo-linear” filter with spatial translation symmetry, a consequence of the convolutional architecture. This structure, reminiscent of the architecture used by Romano *et. al.* [28], allows us to guarantee arbitrary polynomial accuracy, i.e., imposing that approximation errors decay as $\mathcal{O}(\Delta x^m)$ for some power $m \leq N - \ell$, by layering a fixed affine transformation (see appendix). We found the best results with only imposing linear accuracy (i.e., $m = 1$) with a 6-point stencil, which we used for all results shown in this paper. Lastly, the pseudo-linear form is interpretable by construction, as the stencil can be expanded in a Taylor series.

Example coefficients predicted from our trained model are shown in Fig. 2. It is seen that predicted coefficients vary widely within the solution, especially in the vicinity of the shock. In flat regions the coefficients resemble the baseline centered scheme with large kernels, while in the vicinity of the shock they resemble one-sided or short-kernel schemes (Fig. 2 inset). This is in contrast to standard finite-difference schemes which use a single fixed set of coefficients for all points in space.

a. Coarse-graining Ultimately, the goal of the network is to reproduce the “true” high resolution dynamics on a coarse grid. There are two natural ways to understand this goal: the result of the calculation on a coarse grid point can correspond either to the pointwise value of the field in that point (coarse-graining by sub-sampling) or to its mean (coarse-graining by averaging). In this work we take the latter definition. That is, when we refer to the “true” value of the field on a coarse-grid point, we mean the spatial average of the high-resolution field over a coarse grid cell. We also succeeded in coarse-graining by sub-sampling, but to a lesser extent because subsampled dynamics can violate the continuity assumption of Eq. (6). These results are not reported here for brevity.

b. Choice of loss. In machine-learning jargon, the “loss” of a neural net is the objective function which is minimized during training and is supposed to quantify how well the network is performing the given task. There is some freedom in this quantification. Rather than measuring performance by the prediction accuracy of the spatial derivatives directly, we chose to train our model to

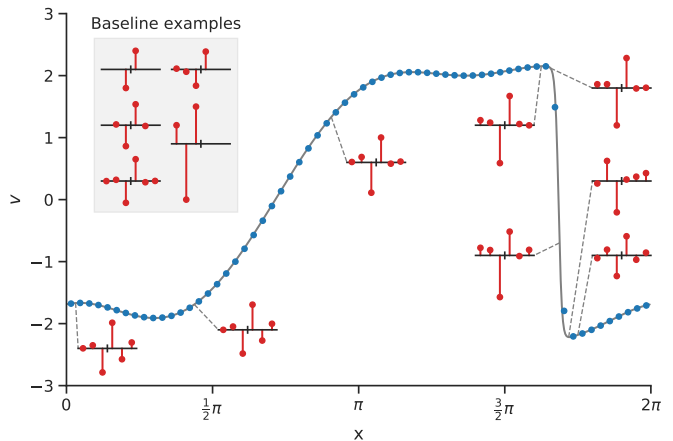


FIG. 2. **Learned finite difference coefficients for a solution to Burgers’ equation.** An example temporal snapshot of a solution to Burgers’ equation Eq. (5). In various points in space we plot the finite difference coefficients, $\alpha_1, \dots, \alpha_6$ (see Eq. (7)) for $\partial v/\partial x$ predicted based on the function values in the vicinity of the indicated position. The vertical scale, which is the same for all coefficient plots, is not shown for clarity. It is seen that the learned coefficients vary widely within the solution, especially in the vicinity of the shock. Inset: A few examples of baseline (standard finite-difference) coefficients for approximating $\partial v/\partial x$. The left column shows centered coefficients with kernel sizes of 2, 4, 6 and the right column shows one-sided coefficients.

maximize the estimation accuracy of the resulting time derivative. This allows the minimization process to misrepresent some features of the spatial derivatives, as long as these errors do not manifest themselves in the final temporal derivative. In addition, we incorporated a relative error term in the loss to ensure that our estimates of the temporal derivatives strictly dominate finite differences estimates, rather than focusing on reducing the error for the cases with the highest discrepancy.

RESULTS

To assess the accuracy of the time integration from our coarse grained model, we computed “exact” solutions to Eq. (5) for different realizations of random forcing at high enough resolution such that the solution is fully converged. Then, for the same realization of the forcing we solved the equation at lower resolution. We compare two different schemes: in the first, the spatial derivatives are given by standard finite difference formulas. This simply means that we solve the equation at a lower, possibly underresolved, resolution; in the second method derivatives are estimated by the neural network. Define the gain in spatial resolution, the *resample factor*, as the ratio between the number of grid points in the low resolution

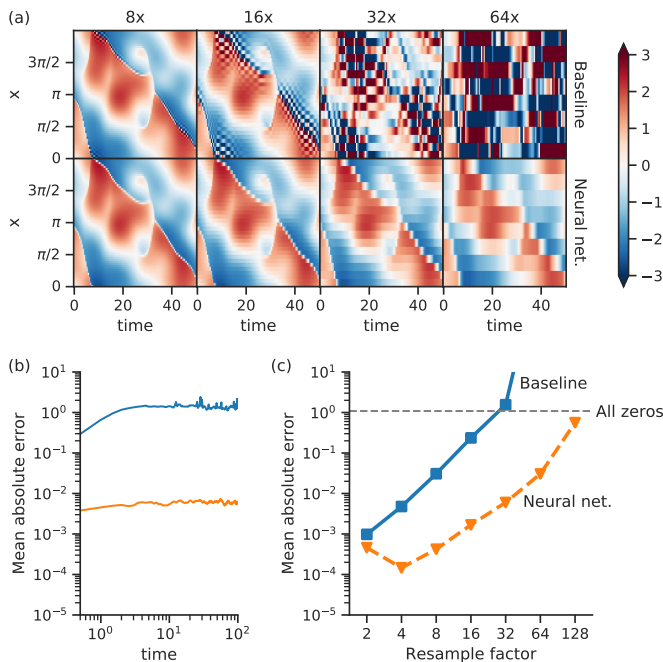


FIG. 3. **Integration results for Burgers' equation.** (a) A particular realization of the solution at varying resolution solved by the baseline finite volume method (top row) and the neural network (bottom row). The neural net method manifestly outperforms the baseline method. (b) Mean Absolute Error (MAE) averaged over many forcing realizations for the 32x resampled simulations, as a function of time. The error saturates at approximately $t = 3$. (c) MAE averaged over many forcing realizations and over time, as a function of resampling factor. Note that the MAE is normalized such that the a prediction of a all zeros corresponds to MAE of unity (see Methods for details).

calculation and that of the fully converged solution¹. Results are shown in Fig. 3: Panel (a) compares the neural network and finite difference solutions for a particular realization of the forcing. It is seen that not only can the neural net integration propagate the solution in time, it dramatically outperforms finite difference method at low resolution. Importantly, the ringing effect around the shocks, which leads to numerical (and unphysical) instabilities, is practically eliminated. Averaging over many realizations of the forcing, it is seen in panels (b) and (c) that the error between the neural net integration and the exact solution saturates over time at a value which is orders of magnitude lower than the baseline. The solution from the neural network has equivalent accuracy to

¹ Physically, the natural measure of the spatial resolution is with respect to the internal length-scale of the equation which in the case of Burgers' equation is the typical shock width. However, since this analysis is meant to be applicable also to situations where the internal lengthscale is a-priori unknown, we compare here the to the lengthscale at which mesh convergence is obtained.

increasing the resolution for finite differences by a factor of 4-8x.

This calculation demonstrates that the neural network is able to carry out coarse graining: even if the mesh spacing is much larger than the shock width the network still is able to accurately propagate the dynamics, demonstrating that it has learned an internal representation of the shock structure to an extent that allows propagating solutions in time.

OTHER EXAMPLES

To demonstrate the robustness of this method, we repeated the procedure for two other canonical PDEs in mathematical physics: The Kuramoto-Sivashinsky (KS) equation, which models flame fronts and is a textbook example of a classically chaotic PDE [29]; and the Korteweg-de Vries (KdV) equation [30], first derived to model solitary waves on a river bore and also a canonical one dimensional PDE known for being completely integrable and to feature soliton solutions:

$$\text{KS : } \frac{\partial v}{\partial t} + \frac{\partial^4 v}{\partial x^4} + \frac{\partial^2 v}{\partial x^2} + \frac{1}{2} \left(\frac{\partial v}{\partial x} \right)^2 = 0 \quad (8)$$

$$\text{KdV : } \frac{\partial v}{\partial t} + \frac{\partial^3 v}{\partial x^3} - 6v \frac{\partial v}{\partial x} = 0. \quad (9)$$

For each of the equations we repeated the training procedure outlined above: First, high resolution simulation were run at a spatial resolution small enough to achieve mesh convergence. The collected data was used to train equation-specific estimators of the spatial derivative based on a coarse grid. Finally, the trained network was used to integrate the equation in time. Note that for these equations, being essentially non-dissipative, we do not include a forcing term. The solution manifold is explored by changing the initial conditions, which are taken to be a superposition of long-wavelength sinusoidal functions with random amplitudes and phases.

In order to assess the accuracy of the integrated solution, for each realization of the initial condition we define the “valid simulation time” as the first time that the low-resolution integrated solution deviates from the true high-resolution solution by more than a given threshold. We found it was more informative to compare this across very different equations than absolute error. In Fig. 4 we plot the median valid simulation time as a function of the resample factor. For all equations, at low resample factor the neural net performs as well as the baseline, since the resolution is fine enough to have mesh convergence and the baseline solution is essentially exact. At higher resample factors the finite-difference scheme deviates more rapidly from the true solution than the neural network, demonstrating a considerable improvement of the neural net scheme over the baseline finite-difference method. Finally, at large enough resample factors the neural network approximations also fails to reproduce the

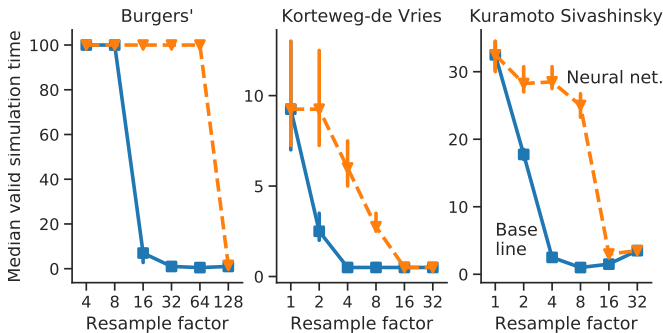


FIG. 4. **Baseline (finite volume) versus neural network simulation results for each of our test equations.** Each plot shows the time for which an integrated solution remains “valid” for each model, defined by the absolute error on at least 80% of grid points being less than the 20th percentile of the absolute error from predicting all zeros. These thresholds were chosen so that “valid” corresponds to relatively generous definition of an approximately correct solution. Error bars show the 95% confidence interval for the median across 100 simulations for each equation, determined by bootstrap resampling. Note that the simulations of Burgers’ equation were run out to a maximum of time of 100. The “exact” solutions for KdV and KS were computed with a spectral method, which explains why they do not exactly match the baseline at 1x resolution.

dynamics, as expected. Figures illustrating these results for specific realizations of each of these equations can be found in the appendix.

DISCUSSION AND CONCLUSION

It has long been remarked that even simple nonlinear partial differential equations can generate solutions of great complexity. But even very complex, possibly chaotic, solutions are not just arbitrary functions, they are highly constrained by the equations that they solve. Nonlinear PDEs have local features that interact over time in a complicated fashion. It has been common to identify these features and describe their interaction with dynamical rules that have been well studied over the past fifty years. Examples include, among many others, interactions of shocks in complex media, interactions of solitons [30], or the turbulent energy cascade [31].

Machine learning offers a different approach for modeling these phenomena, learning both the features and their interactions from experience. In this paper we propose a simple algorithm for achieving this, motivated by coarse graining in physical systems. There, it is often the case that coarse graining a PDE amounts to modifying the weights in a discretized numerical scheme. Instead, we use known solutions to learn these weights directly, generating *data driven discretizations*. This effectively parameterizes the solution manifold of the partial differential equation, allowing the equation to be solved at high accuracy with an unprecedented low resolution.

Faced with this success, it is tempting to ask whether it is possible to leverage the understanding that the neural network has developed – encoded in the learned convolutional filters – to gain new insights about the equation or its coarse-grained representation. For example, could we extract from the trained weights some properties of the shocks, like the typical relations between their height and width? Despite numerous attempts, we were not successful in doing so. It is not easy to directly explore relations between abstract notions such as “shock” or “length scale” since the network internally represents, at least in the shallowest layer, only pointwise values of the field. Indeed, extracting meaningful insights from trained networks is a difficult problem in general, under intensive current research [32–34].

Lastly, while the results presented above are promising, several challenges need to be resolved before data-driven discretization can be deployed at large scales. The first challenge is speed. In this work we used neural networks, due to their flexibility. However, this means that when integrating the equation at each time step many more convolution operations are required than the single convolution required to implement finite differences, e.g., $32^2 = 1024$ convolutions with a five point stencil between our second and third convolutional layers. While this work directly proves the possibility of efficient discretization, we do not believe that our specific implementation is optimal. Indeed, recent work on a closely related problem – inferring sub-pixel resolution data from natural images – has implemented pseudo-linear filters directly, without a convolutional net, enabling much faster inference [28]. The basic idea behind their algorithm is to divide the input image into local patches, classify the patches according to some property (in their work this is the curvature), and learn a linear filter for each class by standard least-squared method. This reduces inference to calculating the local curvature and applying a curvature-specific linear filter. In the future we plan to explore a similar implementation of data-driven discretization, that would allow deployment of this method in large scale simulations. In addition to speed, it is expected to yield a computational architecture which would make it easier to extract physical insights from the trained filters.

The second challenge is dimensionality. Here we have showcased the method for discretizing space in one dimension, but most problems in the real world are of a higher dimension. We expect larger potential gains in two and three dimensions, as the computational gain in terms of the number of grid points would scale like the square or the cube of the resample factor. Indeed, there is every reason to believe that a similar approach would be able to describe patterns higher dimensions, be it hurricanes over the ocean, plumes in chemical reactions or turbulent convection.

A final challenge is handling irregular and adaptive grids, as often used with finite element methods. Adaptive grids are in some ways the most similar in spirit of standard numerical methods to data-driven discretiza-

tion. Similar to what we found here, we expect that hand-tuned heuristics for both gridding and grid coefficients could be improved upon by systematic machine learning. We note that deep learning methods have been developed both for handling the structure of arbitrary graphs [35] and collections of points in 3D space [36].

When these problems are solved, data driven discretizations will offer a possible route towards efficiently solving problems never before accessible with current computational power.

METHODS

c. Neural network details Complete source code, allowing production of a training dataset, training the network on it, and deployment of the resulting coarse-grained equation is freely available online [25]. Our model was implemented using the TensorFlow library [37]. In the calculations presented here, the model had three fully convolutional layers, each with 32 filters of a fixed kernel of size five and with a ReLU nonlinearity between each layer. The code allows to easily tune these hyper parameters.

We trained our models using the Adam optimizer for 40,000 steps total, half with a learning rate of 1×10^{-3} and half with 1×10^{-4} . We used a batch size of 128 times the resampling factor. Each of our models trained to completion in less than an hour on a single Nvidia P100 GPU.

For our loss, we use a linear combination of exact and relative squared error at each point,

$$\alpha(y - \hat{y})^2 + \beta \frac{(y - \hat{y})^2}{(y - \tilde{y})^2 + \gamma} \quad (10)$$

where y denotes the true value of a partial derivative (e.g., $\partial v / \partial t$ or $\partial v / \partial x$) from a high resolution simulation

(spatially averaged over a grid cell), \hat{y} denotes the neural network estimate, \tilde{y} denotes the baseline solution from first-order finite-differences, and α , β and γ are model hyper-parameters. In this work, we set γ to the 10th percentile of $(y - \tilde{y})^2$, and adjusted α and β so that a prediction of all zeros would correspond to an exact and relative squared error of 1/2 each. To calculate the overall loss, we combined losses for both time derivative $\partial v / \partial t$ and all relevant spatial derivatives (e.g., $\partial v / \partial x$), given the time derivative a weight of 0.99 and all space derivatives a weight of 0.01.

d. Training data To train the network we generate a set of 8000 high-resolution solutions to each equation. All equations discussed here employed periodic boundary conditions. Burgers' equation [Eq. (5)] was solved over the range $x \in [0, 2\pi)$ with $\eta = 0.04$; KdV and KS were solved over the ranges $x \in [0, 32)$ and $x \in [0, 64)$, respectively. The forcing in Burgers' equation is a sum of time-varying sinusoidal waves at large wavelength with random amplitude and phase. For KS and KdV there is no forcing and diverse solutions are obtained using different initial conditions which are, again, a sum of random long-wavelength sinusoidal functions. To obtain high accuracy "exact" solutions, we used first-order Finite Volumes for Burgers' equation (due to its characteristic shocks) and a spectral method for KdV and KS.

ACKNOWLEDGMENTS

We thank Peyman Milanfar, Pascal Getreuer and Ignacio Garcia Dorado for collaboration and important conversations, and Peter Norgaard and Geoff Davis for feedback on drafts of the manuscript. Y.B.S. acknowledges support from the James S. McDonnell post-doctoral fellowship for the study of complex systems. M.P.B. acknowledges support from NSF DMS-1715477 as well as the Simons Foundation.

-
- [1] J. D. Jackson, *Classical Electrodynamics* (John Wiley & Sons, 1999).
 - [2] D. Sholl and J. A. Steckel, *Density functional theory: a practical introduction* (John Wiley & Sons, 2011).
 - [3] C. J. Chen, *Fundamentals of turbulence modelling* (CRC Press, 1997).
 - [4] M. Van Dyke, NASA STI/Recon Technical Report A 75 (1975).
 - [5] I. G. Kevrekidis and G. Samaey, *Annual Review of Physical Chemistry* **60**, 321 (2009).
 - [6] P. J. Schmid, *Journal of Fluid Mechanics* **656**, 5 (2010).
 - [7] J. H. Tu, C. W. Rowley, D. M. Luchtenburg, S. L. Brunton, and J. N. Kutz, *Journal of Computational Dynamics* **1**, 391 (2014).
 - [8] M. Schmidt and H. Lipson, *Science* **324**, 81 (2009).
 - [9] S. L. Brunton, J. L. Proctor, and J. N. Kutz, *Proceedings of the National Academy of Sciences* **113**, 3932 (2016).
 - [10] B. Kim, V. C. Azevedo, N. Thuerey, T. Kim, M. Gross, and B. Solenthaler, *arXiv Preprint 1806.02071* (2018).
 - [11] J. Tompson, K. Schlachter, P. Sprechmann, and K. Perlin, *arXiv Preprint 1607.03597* (2016).
 - [12] P. Gentine, M. Pritchard, S. Rasp, G. Reinaudi, and G. Yacalis, *Geophysical Research Letters* (2018).
 - [13] Y. Xie, E. Franz, M. Chu, and N. Thuerey, *ACM Transaction on Graphics (SIGGRAPH)*, *arXiv Preprint 1801.09710* (2018).
 - [14] E. de Bezenac, A. Pajot, and P. Gallinari, in *International Conference on Learning Representations* (2018).
 - [15] B. Lusch, J. N. Kutz, and S. L. Brunton, *arXiv Preprint 1712.09707* (2017).
 - [16] J. Morton, F. D. Witherden, A. Jameson, and M. J. Kochenderfer, *arXiv Preprint: 1805.07472* (2018).
 - [17] J. Ling, A. Kurzawski, and J. Templeton, *Journal of Fluid Mechanics* **807**, 155 (2016).

- [18] A. D. Beck, D. G. Flad, and C.-D. Munz, [arXiv Preprint 1806.04482](#) (2018).
- [19] W. E. Schiesser, *The numerical method of lines: integration of partial differential equations* (Academic Press San Diego, San Diego, 1991).
- [20] A. Harten, B. Engquist, S. Osher, and S. R. Chakravarthy, in *Upwind and high-resolution schemes* (Springer, 1987) pp. 218–290.
- [21] P. Getreuer and F. G. Meyer, *SIAM Journal on Numerical Analysis* **46**, 2953 (2008).
- [22] M. Lee and R. D. Moser, *Journal of Fluid Mechanics* **774**, 395 (2015).
- [23] M. Clay, D. Buaria, T. Gotoh, and P. Yeung, *Computer Physics Communications* **219**, 313 (2017).
- [24] K. P. Iyer, K. R. Sreenivasan, and P. K. Yeung, *Physical Review E* **95**, 021101 (2017).
- [25] <https://github.com/google/pde-superresolution>.
- [26] I. Goodfellow, Y. Bengio, A. Courville, and Y. Bengio, *Deep learning* (MIT press Cambridge, 2016).
- [27] S. Mazumder, *Numerical methods for partial differential equations: finite difference and finite volume methods* (Academic Press, London, 2016).
- [28] Y. Romano, J. Isidoro, and P. Milanfar, *IEEE Transactions on Computational Imaging* **3**, 110 (2017).
- [29] D. Zwillinger, *Handbook of differential equations* (Gulf Professional Publishing, 1998).
- [30] N. J. Zabusky and M. D. Kruskal, *Physical Review Letters* **15**, 240 (1965).
- [31] U. Frisch, *Turbulence: The Legacy of A. N. Kolmogorov* (Cambridge University Press, 1996).
- [32] D. Baehrens, T. Schroeter, S. Harmeling, M. Kawanabe, K. Hansen, and K.-R. Müller, *Journal of Machine Learning Research* **11**, 1803 (2010).
- [33] M. Sundararajan, A. Taly, and Q. Yan, [arXiv Preprint 1703.01365](#) (2017).
- [34] A. Shrikumar, P. Greenside, and A. Kundaje, [arXiv Preprint 1704.02685](#) (2017).
- [35] J. Gilmer, S. S. Schoenholz, P. F. Riley, O. Vinyals, and G. E. Dahl, in *Proceedings of the 34th International Conference on Machine Learning*, Proceedings of Machine Learning Research, Vol. 70, edited by D. Precup and Y. W. Teh (PMLR, International Convention Centre, Sydney, Australia, 2017) pp. 1263–1272.
- [36] C. R. Qi, L. Yi, H. Su, and L. J. Guibas, in *Advances in Neural Information Processing Systems*, Vol. 30 (2017).
- [37] M. Abadi, P. Barham, J. Chen, Z. Chen, A. Davis, J. Dean, M. Devin, S. Ghemawat, G. Irving, M. Isard, M. Kudlur, J. Levenberg, R. Monga, S. Moore, D. G. Murray, B. Steiner, P. Tucker, V. Vasudevan, P. Warden, M. Wicke, Y. Yu, and X. Zheng, in *12th USENIX Symposium on Operating Systems Design and Implementation (OSDI 16)* (2016) pp. 265–283.
- [38] B. Fornberg, *Mathematics of computation* **51**, 699 (1988).
- [39] F. Pedregosa, G. Varoquaux, A. Gramfort, V. Michel, B. Thirion, O. Grisel, M. Blondel, P. Prettenhofer, R. Weiss, V. Dubourg, J. Vanderplas, A. Passos, D. Cournapeau, M. Brucher, M. Perrot, and E. Duchesnay, *Journal of Machine Learning Research* **12**, 2825 (2011).

APPENDIX I: POLYNOMIAL ACCURACY CONSTRAINTS

Our method represents the spatial derivative at a point x_0 as a linear combination of the function values at N neighbors of x_0 . That is, for a given derivative order ℓ , we write

$$\left. \frac{\partial^\ell f}{\partial x^\ell} \right|_{x=x_0} = \sum_{n=1}^N \alpha_n f(x_0 + h_n) \quad (\text{S-1})$$

where h_n is the offset of the n -th neighbor on the coarse grid. Note that in the main text we only deal with uniformly spaced meshes, $h_n = n \Delta x$, but this formalism holds for an arbitrary mesh. A crucial advantage of this writing is that we can enforce arbitrary polynomial accuracy up to degree m , as long as $m \leq N - \ell$, by imposing an affine constraint on the α 's. That is, we can ensure that the error in approximating $f^{(\ell)}$ will be of order h^m for some $m \leq N - \ell$.

To see this, note that the standard formula for deriving the finite difference coefficients for the ℓ -th derivative with an N -point stencil is obtained by solving the linear set of equations [38]:

$$\begin{pmatrix} h_1^0 & \cdots & h_N^0 \\ \vdots & \ddots & \vdots \\ h_1^{N-1} & \cdots & h_N^{N-1} \end{pmatrix} \begin{pmatrix} \alpha_1 \\ \vdots \\ \alpha_N \end{pmatrix} = \ell! \begin{pmatrix} \delta_{0,\ell} \\ \vdots \\ \delta_{i,\ell} \\ \vdots \\ \delta_{N-1,\ell} \end{pmatrix} \quad (\text{S-2})$$

where $\delta_{i,j}$ is the Kronecker delta. These equations are obtained by expanding Eq. (S-1) in a Taylor series up to order $m - 1$ in the vicinity of x_0 and requiring equality of order $\mathcal{O}(h^m)$ for arbitrary functions. Each row in the set of equations corresponds to demanding that a term of order h^k will vanish, for $k = 0, 1, \dots, N-1$. The resulting formula is approximate to polynomial order $N - \ell$ [38] and the system of equation is fully determined, that is, a unique solution exists, which is obtained by inverting the matrix.

Imposing a lower order approximation amounts to removing the bottom rows from the equation Eq. (S-2). Specifically, imposing accuracy of order m amounts to keeping the first $m - N + \ell$ rows, which makes the system under-determined. Therefore, any solution for α can be written as a sum of an arbitrary fixed solution (say, the standard-finite difference formula of order m) plus a vector $\tilde{\alpha}$ from the null-space of the matrix of Eq. (S-2) (with removed rows).

APPENDIX II: SUPPORT VECTOR REGRESSION

The regression presented in Fig. 1 of the main text was obtained in the following way: First, training data was generated by running 100 high resolution simulations of Burgers' Equation and sampling them at regular intervals. Then, each sampled snapshot was cut into non-overlapping segments of length $5 \times$ resample factor, which for the case of Fig. 1 was 5. From the complete dataset, 30,000 segments were randomly chosen for training, with probability proportional to the average curvature of a segment, thus giving more weight to shocks than to flat regions. The examples shown in Fig. 1 were not in the training set. On this training set the regression problem is defined by predicting the high-resolution field (vector of length 25) from the low resolution subsampled field (vector of length 5). This regression problem was solved using the NuSVR function from the open-source package scikit-learn [39], with parameters $\nu = 4 \times 10^{-3}$ and $C = 10$.

APPENDIX III: RESULTS FOR KDV AND KS EQUATIONS

Similar to panel (a) of Fig. 2 in the main text, we show in Figures S1 and S2 one particular realization of solutions to the KdV and KS Equations, respectively. The figures show how the same initial condition is solved at different resample factors by the baseline finite-difference method and neural network, demonstrating that our method significantly outperforms the baseline.

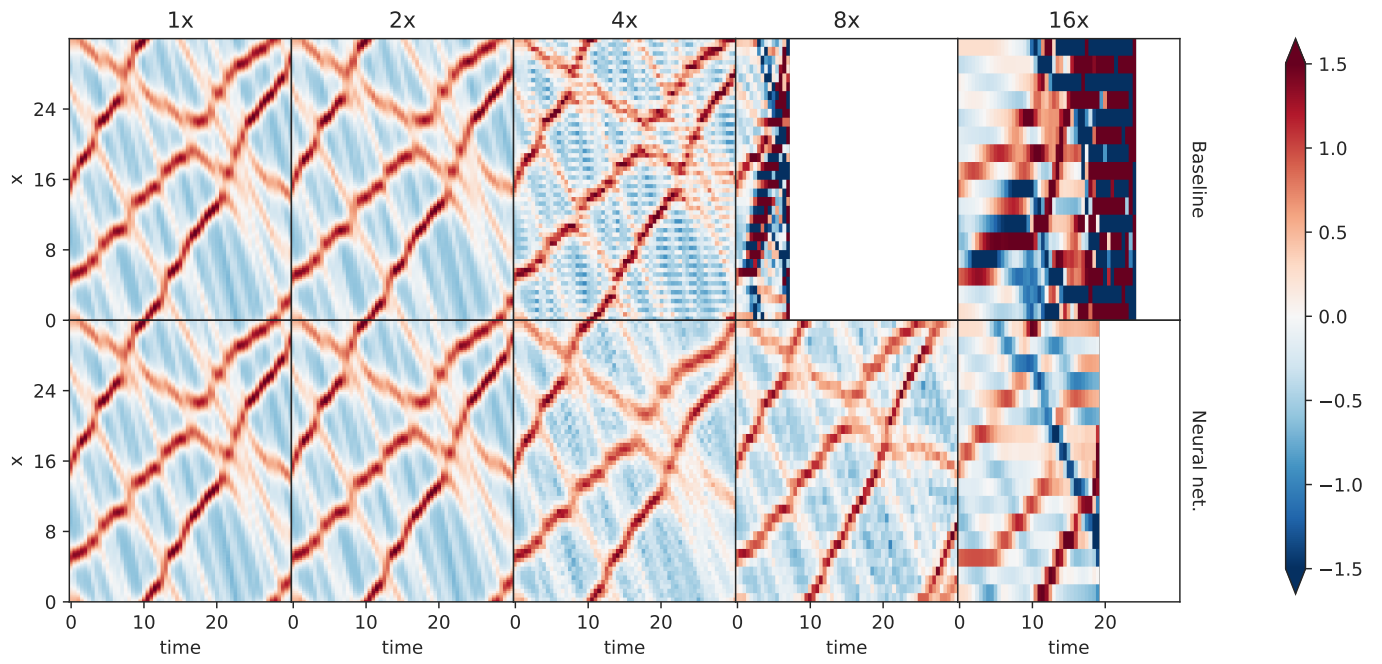


FIG. S1. Particular realization of the solution for the Korteweg-de Vries (KdV) equation at varying resolution solved by the baseline finite volume method (top row) and the neural network (bottom row). Blank regions indicate where the solver has diverged.

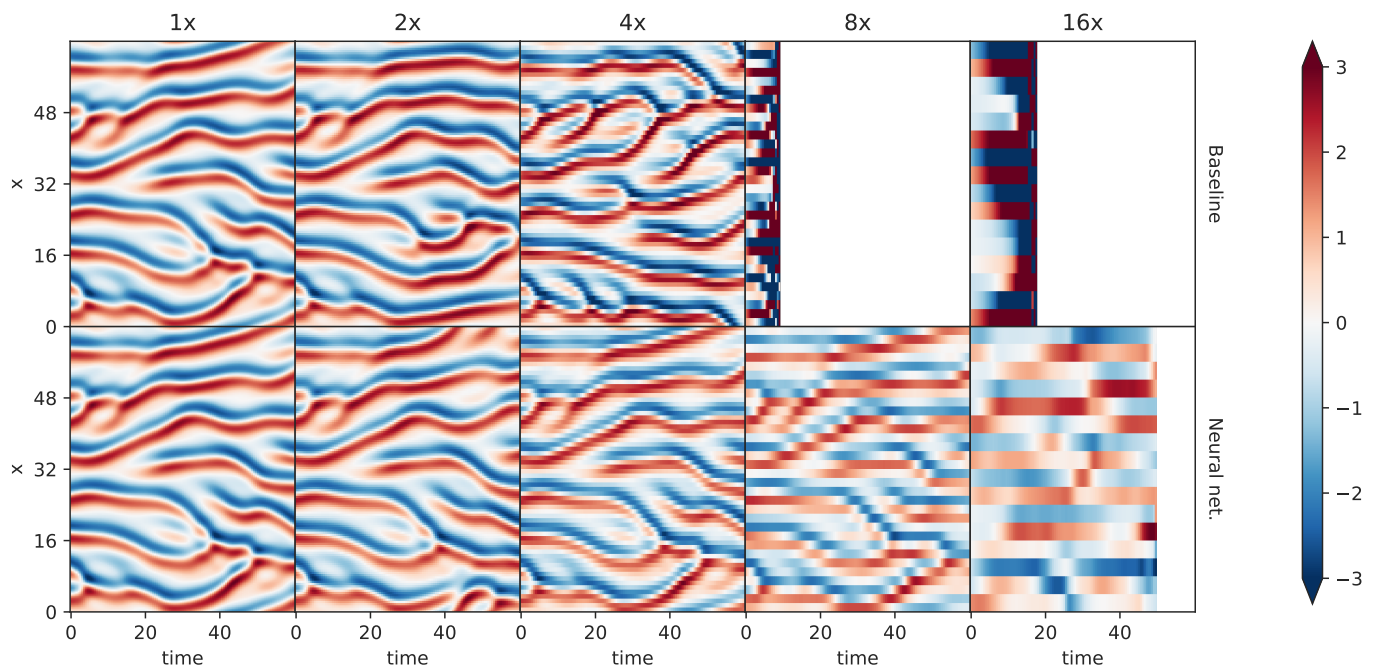


FIG. S2. Same as S1, but for the Kuramoto-Shivashinsky (KS) equation.